Characterizing the Robustness of a Physics-Informed Model for Anisotropic Conduction and Fiber Orientation Estimation in Atrial Tissue

Stephanie Appel[1], Tobias Gerach[1], Cristian Barrios Espinosa[1], Christian Wieners[2], Axel Loewe[1]

[1] Institute of Biomedical Engineering, Karlsruhe Institute of Technology (KIT), Karlsruhe, Germany
[2] Institute of Applied and Numerical Mathematics, KIT, Karlsruhe, Germany

Abstract

Estimating heterogeneous conduction velocities (CVs) in the atria is essential for understanding arrhythmia mechanisms but remains challenging due to sparse and noisy clinical data. FiberNet, a physics-informed neural network-based method, offers a data-efficient approach to estimate direction-dependent CVs and fiber orientation from local activation time maps.

We present a synthetic 2D benchmark setup, physiologically motivated by atrial tissue properties, specifically the preferential orientation of cardiomyocytes, as well as region-specific CVs and anisotropy ratios. By systematically varying data quality and fiber complexity, we analyzed FiberNet's robustness and accuracy in estimating anisotropic properties across heterogeneous tissue, accounting for anatomical variability.

Performance was evaluated using error thresholds of 30° for fiber angle (α) and 0.1 m/s and 0.2 m/s for CV. For uniform or sharply heterogeneous tissues, predictions were within these thresholds for 86 % (α), 67 % (CV, 0.1 m/s), and 79 % (CV, 0.2 m/s). Under Gaussian noise ($\sigma = 1$ m/s) percentages decreased to 61 %, 24 %, and 44 %, respectively. In regions with gradual fiber transitions, only 67 % of α predictions remained below 30°. These results highlight conditions of reliable performance and opportunities for targeted improvement to advance clinical impact.

1. Introduction

Conduction velocity (CV) reflects how fast electrical signals travel through cardiac tissue. Due to the heart tissue's anisotropic structure, shaped by the preferential orientation of cardiomyocytes, CV varies directionally and spatially due to heterogeneity, influencing activation patterns. Pathological remodeling can slow CV and promote conduction heterogeneity, contributing to the arrhythmogenic substrate of atrial fibrillation [1]. Mapping direction-dependent CV can thus improve mechanistic understanding and support personalized treatment strategies. Gradient-based approaches estimate CV from spatial and temporal differences in local activation time (LAT) measurements obtained from electro-anatomical mapping [2]. However, the atria's complex geometry, limited resolution and noise inherent to these maps, compromise the accurate reconstruction of anisotropic tissue properties. These challenges have motivated the use of other modeling approaches. Among these methods, physics-informed neural networks (PINNs) combine the flexibility of deep learning with physical constraints, offering a potential solution to infer conduction properties from sparse and noisy LAT maps. Building on a PINN-based approach [3], FiberNet [4] estimates spatially varying, anisotropic tissue properties from LAT maps. Since then, it has been refined to enhance accuracy and robustness [5].

In this study, we present a controlled, physiologically inspired in-silico framework to evaluate CV estimation method prediction accuracy and apply it to FiberNet.

2. Material and Methods

2.1. Propagation Model

Electrical activation in cardiac tissue can be modeled at various levels of complexity [6]. When focusing on activation patterns rather than temporal voltage dynamics, simplified models like the anisotropic eikonal equation can be used [7]. This model describes the propagation of electrical wavefronts while accounting for tissue anisotropy:

$$\sqrt{\nabla\phi(\boldsymbol{x})^\top \boldsymbol{D}(\boldsymbol{x})\nabla\phi(\boldsymbol{x})} = 1 \quad \forall \boldsymbol{x} \in \Omega \subseteq \mathbb{R}^3, \tag{1a}$$

$$\phi(\boldsymbol{x}) = \phi_0 \quad \forall \boldsymbol{x} \in \Gamma_0 \subset \Omega, \tag{1b}$$

where for each location $\boldsymbol{x}$ in a domain Ω, the positive-definite, symmetric tensor $\boldsymbol{D}(\boldsymbol{x})$ defines the conduction properties, and $\phi(\boldsymbol{x})$ is the activation time of a cell in $\boldsymbol{x}$, for a propagating wave initiated in Γ_0 at time ϕ_0.

The atria are often modeled as a surface $\mathcal{S} \subseteq \Omega$, ignoring a propagation perpendicular to $\mathcal{S}$. Given this assumption, $\boldsymbol{D}(\boldsymbol{x})$ defines the direction-dependent conduc-

tion properties of the cardiac tissue and can be written as

$$\boldsymbol{D}(\boldsymbol{x}) = \mathrm{CV}_{\parallel}^2(\boldsymbol{x})\boldsymbol{l}(\boldsymbol{x}) \otimes \boldsymbol{l}(\boldsymbol{x}) + \mathrm{CV}_{\perp}^2(\boldsymbol{x})\boldsymbol{t}(\boldsymbol{x}) \otimes \boldsymbol{t}(\boldsymbol{x}) \quad \forall \boldsymbol{x} \in \mathcal{S} \subseteq \Omega \tag{2}$$

with

$$\boldsymbol{l}(\boldsymbol{x}) = \begin{bmatrix} \cos(\alpha(\boldsymbol{x})) \\ \sin(\alpha(\boldsymbol{x})) \\ 0 \end{bmatrix}, \; \boldsymbol{t}(\boldsymbol{x}) = \begin{bmatrix} -\sin(\alpha(\boldsymbol{x})) \\ \cos(\alpha(\boldsymbol{x})) \\ 0 \end{bmatrix}, \tag{3}$$

where $\boldsymbol{l}(\boldsymbol{x})$ and $\boldsymbol{t}(\boldsymbol{x})$ form an orthonormal system representing the local preferential orientation of the cardiomyocytes, corresponding to the longitudinal and transversal directions. $\mathrm{CV}_{\parallel}(\boldsymbol{x})$ and $\mathrm{CV}_{\perp}(\boldsymbol{x})$ correspond to the local conduction velocities in longitudinal and transversal direction, while $\alpha(\boldsymbol{x})$ defines the fiber orientation angle.

2.2. FiberNet

We used the 2D version of FiberNet [4]. Although recent work [5] introduced improvements in surface handling and incorporated uncertainty quantification, the previous version was used due to the availability of the open-source code. In the following, a concise overview of the method is provided. For further details, we refer to [4].

FiberNet is a PINN framework for estimating cardiac conduction properties from sparse LAT data. Given LAT samples on a known surface, it predicts full LAT maps and the underlying direction-dependent conduction features, by incorporating the eikonal equation as a biophysical constraint into the learning process.

Formally, for a given surface geometry $\mathcal{S}$ with spatial coordinates $\boldsymbol{x} \in \mathcal{S} \subseteq \mathbb{R}^3$, we denote the LATs $\phi_i(\boldsymbol{x}_k)$, where $i = 1, ..., N$ indexes the LAT maps and $k = 1, ..., N_i$ the sampled points per map. FiberNet predicts the LAT maps $\hat{\phi}_i(\boldsymbol{x})$ and the squared CV tensor $\hat{\boldsymbol{D}}(\boldsymbol{x})$ defined by $\hat{\mathrm{CV}}_{\parallel}(\boldsymbol{x})$, $\hat{\mathrm{CV}}_{\perp}(\boldsymbol{x})$, and $\hat{\alpha}(\boldsymbol{x})$.

The architecture consists of separate neural networks for LAT map predictions (5 hidden layers, 10 neurons each, and weights θ_ϕ) and another one for tissue property estimation (5 hidden layers, 5 neurons each, and weights $\theta_{\boldsymbol{D}}$). For training, we used 245 sample points, evenly distributed across N LAT maps, to minimize the total loss function

$$\mathcal{L}(\theta_{\boldsymbol{D}}, \theta_\phi) = \lambda_{\mathrm{data}}\mathcal{L}_{\mathrm{data}}(\theta_\phi) + \lambda_{\mathrm{eiko}}\mathcal{L}_{\mathrm{eiko}}(\theta_{\boldsymbol{D}}, \theta_\phi) + \lambda_{\mathrm{CV}}\mathcal{L}_{\mathrm{CV}}(\theta_{\boldsymbol{D}}) + \lambda_\alpha\mathcal{L}_\alpha(\theta_{\boldsymbol{D}})\,. \tag{4}$$

The loss comprises four terms, each targeting a different aspect of model performance: (i) Data loss $\mathcal{L}_{\mathrm{data}}$: Penalizes discrepancies between predicted and reference LAT values at sampling locations. (ii) Physics-informed loss $\mathcal{L}_{\mathrm{eiko}}$: Favors consistency with wave propagation dynamics by penalizing deviations from the eikonal equation at collocation points. (iii) Regularization losses $\mathcal{L}_{\mathrm{CV}}$ and $\mathcal{L}_\alpha$: Promote piecewise smoothness in predicted CVs and fiber angle, mitigating the ill-posedness of the inverse problem by promoting physiologically plausible solutions. Relative importance of these terms is controlled by the weight factors $\lambda_{\mathrm{data}} = 1$, $\lambda_{\mathrm{eiko}} = 10^{-2}$, $\lambda_{\mathrm{CV}} = 10^{-5}$, and $\lambda_\alpha = 10^{-9}$.

2.3. Benchmark Setups

We designed synthetic 2D test cases with atria-inspired conduction and fiber patterns. While clinical data lack explicit ground truth, this setup offers a controlled environment for quantitative validation.

Each case is defined on a $2 \times 2\,\mathrm{cm}^2$ tissue patch discretized into a 35×35 grid, accounting for region-specific anisotropic properties through spatially varying fiber orientations and direction-dependent conduction velocities. The setup includes both smoothly varying and abrupt transitions to reflect physiologically relevant heterogeneity. Details of the individual test cases and assigned tissue properties are summarized in Figure 1 and Table 1.

For each test case, we generated LAT maps by solving the anisotropic eikonal equation using the Fast Iterative Method [8], with pacing sites selected by Latin hypercube sampling to diversify activation patterns.

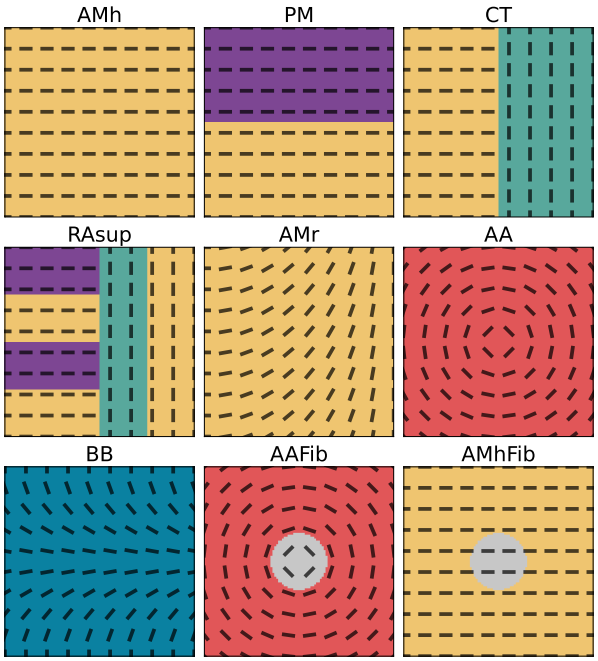

Figure 1. 2D test cases based on atria-inspired tissue patches, with region-specific conduction velocities (see Table 1) and fiber orientations (black lines). AMh/r – atrial myocardium with horizontal/rotated fibers; PM: pectinate muscle; CT – crista terminalis; RAsup – superior right atrium; AA – atrial appendage; BB – Bachmann's bundle; AAFib/AMhFib – AA/AMh with fibrotic core.

Atrial regions	$CV_{\parallel}$ in m/s	$CV_{\perp}$ in m/s
Atrial myocardium	1.2465	0.5905
Atrial appendages	1.2467	0.5950
Crista terminalis	1.6839	0.5911
Pectinate muscles	1.7435	0.4612
Bachmann's bundle	2.1511	0.6450
Fibrosis	0.2000	0.2000

Table 1. Region-specific conduction velocities in longitudinal ($CV_{\parallel}$) and transversal ($CV_{\perp}$) preferential orientation of the cardiomyocytes. Values from Nagel et al. [6].

To assess how noise and electrode sampling affect the prediction of anisotropic tissue properties, we applied the following perturbations to the LAT maps: (i) Gaussian noise with standard deviations $\sigma = 1\,\mathrm{ms}$ or $3\,\mathrm{ms}$ to mimic clinical measurement uncertainty. (ii) Outlier regions were introduced to mimic localized clinical artifacts. We placed four randomly located, non-overlapping clusters per LAT map, with each containing 1 to 50 connected nodes assigned a single, random LAT value. (iii) Sampling density was varied between $-75\,\%$ and $+400\,\%$ to evaluate the effect of data resolution on prediction accuracy.

The resulting data, sampled from one, three, or five LAT maps, were then used as input for the predictions.

2.4. Results

Figure 2 shows the median absolute error (MdAE) for $CV_{\parallel}$, $CV_{\perp}$, and α predictions for all tissue cases and selected noise scenarios, taking 245 sample points from three distinct LAT maps. Performance was best without noise, yielding MdAEs of $0.13\,\mathrm{m/s}$ ($CV_{\parallel}$), $0.03\,\mathrm{m/s}$ ($CV_{\perp}$), and $9\,^{\circ}$ (α). Five LAT maps gave similar accuracy, while using one increased errors by $+0.14\,\mathrm{m/s}$, $+0.19\,\mathrm{m/s}$, and $+15^{\circ}$, respectively.

Focusing on three noise-free LAT maps, predictions were reliable across a wide range of tissue configurations. Error distributions across all configurations are shown in Figure 3. α prediction was accurate in uniform patterns, with $\triangle\alpha_{30} = 99\,\%$, i.e., $99\,\%$ of all nodes among AMh, PM, and AMhFib had absolute error $\leq 30\,^{\circ}$. Regions with fiber transitions (CT, RAsup, AMr, AA, BB, AAFib) led to higher MdAEs. While abrupt changes were generally well captured ($\triangle\alpha_{30} = 99\,\%$) with high error mainly near the boundaries, performance dropped for gradual fiber transitions ($\triangle\alpha_{30} = 69\,\%$). Similarly, CV predictions were reliable in uniformly structured tissues, with low MdAEs and narrow error distributions, as $89\,\%$ ($90\,\%$) of nodes had AEs $\leq 0.1\,\mathrm{m/s}$ ($0.2\,\mathrm{m/s}$) ($\triangle CV_{0.1}$, $\triangle CV_{0.2}$). In heterogeneously structured cases (PM, CT, RAsup, AA/AMhFib), accuracy declined with complexity. In RAsup, for instance, broader CV trends were captured, but finer structures, such as pectinate muscles, were less precisely resolved leading to $\triangle CV_{0.1} = 30\,\%$ and $\triangle CV_{0.2} = 48\,\%$.

Analyzing the model's robustness to noise, sampling density had only minor influence. Gaussian noise especially reduced CV prediction accuracy. (see Figure 3). The impact was moderate at $\sigma = 1\,\mathrm{ms}$ (mean over all cases: $\triangle\alpha_{30} = 61\,\%$, $\triangle CV_{0.1} = 24\,\%$, $\triangle CV_{0.2} = 44\,\%$) but severe at $\sigma = 3\,\mathrm{ms}$ ($\triangle\alpha_{30} = 25\,\%$, $\triangle CV_{0.1} = 2\,\%$, $\triangle CV_{0.2} = 5\,\%$). However, note that due to the patch size, noise with $\sigma = 3\,\mathrm{ms}$ corresponded to $\approx 10\,\%$ noise in the LAT maps. Outlier regions also notably reduced accuracy, although this highly depended on the number of sample points overlapping with these regions. Combined noise and outlier effects overwhelmed the learning. Increas-

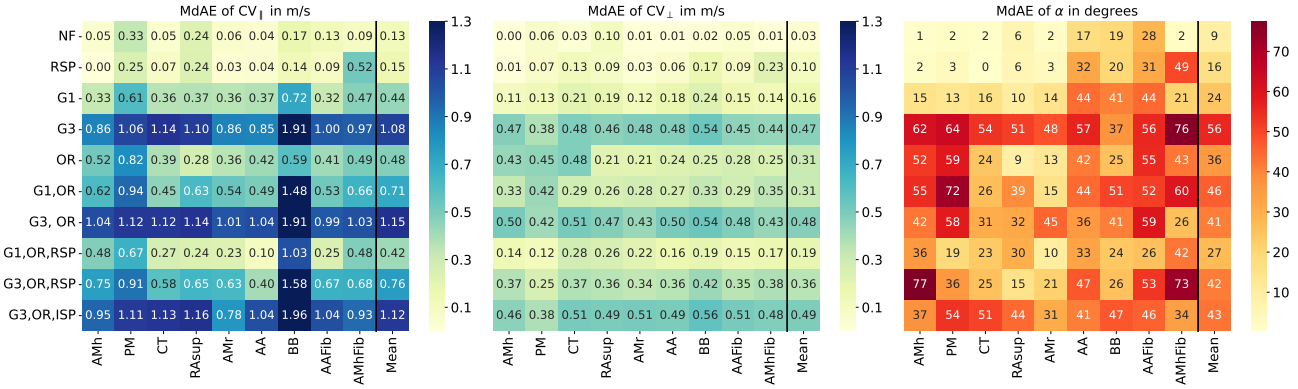

Figure 2. Median absolute error (MdAE) of predicted anisotropic conduction properties - conduction velocities longitudinal ($CV_{\parallel}$) and transversal ($CV_{\perp}$) to fiber orientation, and fiber angle (α) - based on three local activation time (LAT) maps. Comparing prediction accuracy for the cases in Figure 1 (columns), when applying various noise settings to the LAT maps (rows): (i) noise-free (NF), (ii) $400\,\%$ increase or $75\,\%$ reduction of sample points (ISP/RSP), (iii) Gaussian noise with $\sigma = 1\,\mathrm{ms}$ (G1) or $3\,\mathrm{ms}$ (G3) on the LAT maps, (iv) outlier regions (OR), and (v) combinations of these perturbations.

ing sampling density could not compensate for this effect, while reducing it was beneficial.

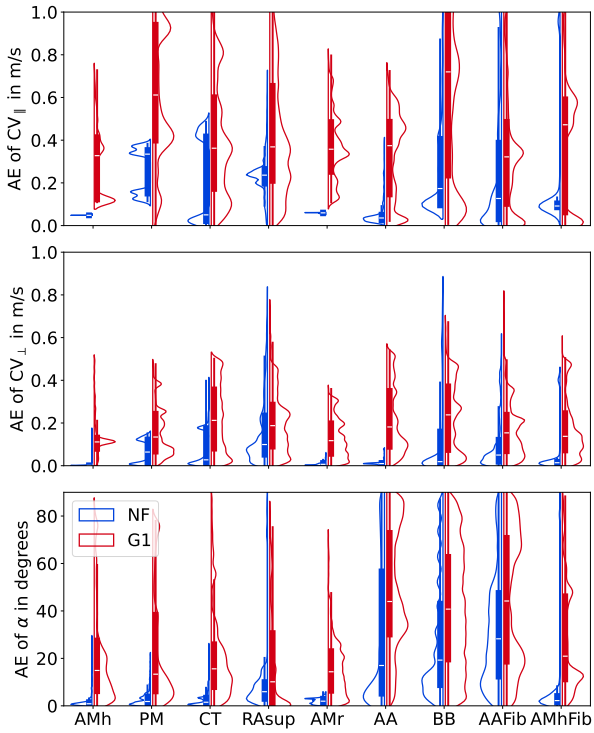

Figure 3. Distribution of absolute error (AE) in predicted anisotropic conduction properties - conduction velocities longitudinal ($CV_{\parallel}$) and transversal ($CV_{\perp}$) to fiber orientation, and fiber angle (α) - based on three local activation time (LAT) maps, noise-free (NF) or with Gaussian noise with $\sigma = 1$ ms (G1), for the cases defined in Figure 1.

3. Discussion

We evaluated FiberNet's ability to predict local tissue properties under varying anatomical complexities and noise levels. In line with the findings in [4], a single LAT map proved insufficient. Multiple LAT maps from distinct pacing sites improved prediction accuracy by providing complementary information on conduction properties, ameliorating the ill-posedness of the inverse problem.

FiberNet provided robust, region-specific CV predictions, especially in uniform or abruptly changing fiber orientations. While sharp transitions were well-captured, boundary regions and gradual fiber transitions presented higher errors. The model showed resilience to sparse sampling, yet Gaussian noise significantly reduced accuracy, particularly for CVs, possibly amplified by the small patch size and limited LAT range.

Median fiber angle predictions remained clinically acceptable ($\leq 30°$), but CV errors in heterogeneous settings often exceeded 0.1 m/s, indicating a need for further optimization. Targeted improvements should focus on enhancing noise robustness and refining performance in gradual fiber transitions, possibly by employing alternative regularization schemes. Future work will extend the framework to 3D atrial geometries for improved analysis and clinical applicability. Furthermore, while surface-defined inputs improve α predictions [5], their benefit for CV remains to be assessed. Ultimately, FiberNet enables more precise, patient-specific characterization of anisotropic conduction properties from sparse data. This capability, representing an enhancement over conventional approaches, holds promise for improving risk stratification and guiding personalized treatment strategies for atrial fibrillation.

Acknowledgments

This research was funded by the Deutsche Forschungsgemeinschaft (DFG, German Research Foundation) – Project-ID 258734477 – SFB 1173.

References

[1] Nattel S, Harada M. Atrial remodeling and atrial fibrillation: recent advances and translational perspectives. J Am Coll Cardiol 2014;63(22):2335–2345.

[2] Coveney S, Cantwell C, Roney C. Atrial conduction velocity mapping: clinical tools, algorithms and approaches for understanding the arrhythmogenic substrate. Med Biol Eng Comput 2022;60(9):2463–2478.

[3] Grandits T, et al. Learning atrial fiber orientations and conductivity tensors from intracardiac maps using physics-informed neural networks. In Functional Imaging and Modeling of the Heart. FIMH. Springer, 2021; 650–658.

[4] Ruiz Herrera C, et al. Physics-informed neural networks to learn cardiac fiber orientation from multiple electroanatomical maps. Eng Comput 2022;38(5):3957–3973.

[5] Magaña E, Pezzuto S, Sahli Costabal F. Ensemble learning of the atrial fibre orientation with physics-informed neural networks. The Journal of Physiology 2025;0.0:1–18.

[6] Nagel C, et al. Comparison of propagation models and forward calculation methods on cellular, tissue and organ scale atrial electrophysiology. IEEE Trans Biomed Eng 2022; 70(2):511–522.

[7] Colli Franzone P, Guerri L, Rovida S. Wavefront propagation in an activation model of the anisotropic cardiac tissue: asymptotic analysis and numerical simulations. J Math Biol 1990;28:121–176.

[8] Fu Z, et al. A fast iterative method for solving the eikonal equation on triangulated surfaces. SIAM J Sci Comput 2011; 33(5):2468–2488.

Address for correspondence:

Stephanie Appel, publications@ibt.kit.edu
Institute of Biomedical Engineering, Karlsruhe Institute of Technology (KIT), Kaiserstr. 12, 76131, Karlsruhe, Germany